J|A|C|S
ARTICLES
Published on Web 02/23/2007

Cyclohexenylphenyldiazene: A Simple Surrogate of the Azobenzene Photochromic Unit

Irene Conti,[†] Filippo Marchioni,[†] Alberto Credi,*[,†] Giorgio Orlandi,[†] Goffredo Rosini,[‡] and Marco Garavelli*[,†]

Contribution from the Department of Chemistry "G. Ciamician", University of Bologna, Via Selmi 2, 40126 Bologna, Italy, and Department of Organic Chemistry "A. Mangini", University of Bologna, Viale del Risorgimento 4, 40136 Bologna, Italy

Received September 22, 2006; E-mail: marco.garavelli@unibo.it; alberto.credi@unibo.it

Abstract: We have carried out an experimental and computational study on the ground- and excited-state photochemical and photophysical properties of (1-cyclohexenyl)phenyldiazene (CPD), a species formally derived from azobenzene in which one of the phenyl rings is replaced by a 1-cyclohexene substituent. The results show that CPD does substantially behave like azobenzene, but with a higher (~70%) $\Phi_{Z\rightarrow E}$ ($n\pi^*$) photoisomerization quantum yield, calling for CPD as an effective alternative of azobenzene itself with new functionalization possibilities. By use of state-of-the-art ab initio CASPT2//CASSCF minimum energy path computations, we have identified the most efficient decay and isomerization routes of the absorbing singlet ($\pi\pi^*$), S_1 ($n\pi^*$), T_1, and S_0 states of CPD. The resulting mechanistic scheme agrees with experimental findings and provides a rationale of the observed photoisomerization quantum yields. Furthermore, this study provides a deep insight on the photophysical and photochemical properties of compounds based on the −N═N− double bond which supplies a general model for the photoreactivity of azobenzene-type compounds in general. This is expected to be a useful guideline for the design of novel photoreactive azo compounds.

1. Introduction

The physicochemical and structural changes associated with the $E \leftrightarrows Z$ photoisomerization of azobenzene derivatives[1−3] have been widely exploited to modify chemical systems by means of light stimulation. For instance, such a reaction has been used to modulate the structural and physicochemical properties of polymers,[4,5] liquid crystals,[6] biomolecules,[7] surfaces,[8] and dendritic[9] and supramolecular[10,11] systems, as well as to construct multichromophoric compounds,[10,12] molecular-level memories,[13] logic gates,[14] devices, and machines.[15,16]

Because of the importance of azobenzene (AB, Chart 1) for both basic science and applicative reasons, the mechanism of its $E \leftrightarrows Z$ photoisomerization reaction has been extensively studied in the past.[1] More recently, owing to the development

Chart 1. Structural Formulas and *E*−*Z* Photochemical and Thermal Isomerization Reactions of Azobenzene (AB) and (1-Cyclohexenyl)phenyldiazine (CPD)

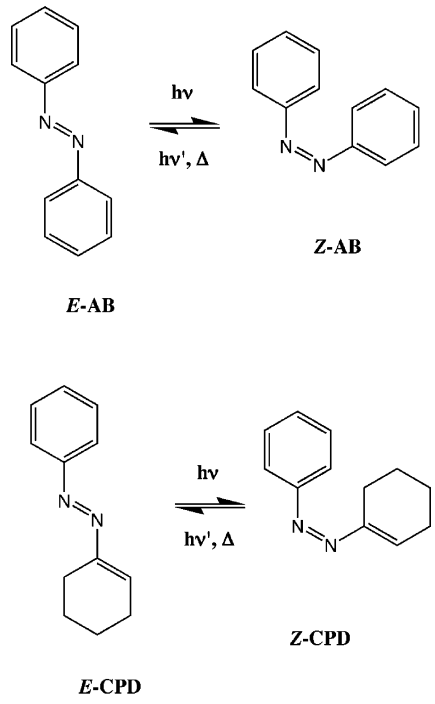

[†] Department of Chemistry "G. Ciamician", University of Bologna.
[‡] Department of Organic Chemistry "A. Mangini", University of Bologna.

(1) Rau, H. In *Photochromism: Molecules and Systems*; Dürr, H., Bouas-Laurent, H., Eds.; Elsevier: Amsterdam, 2003; Chapter 4.
(2) Griffiths, J. *Chem. Soc. Rev.* **1972**, *1*, 481.
(3) Bortolus, P.; Monti, S. *J. Phys. Chem.* **1979**, *83*, 648 and references therein.
(4) (a) Sudesh Kumar, G.; Neckers, D. C. *Chem. Rev.* **1989**, *89*, 1915. (b) Natansohn, A.; Rochon, P. *Chem. Rev.* **2002**, *102*, 4139.
(5) For a recent interesting example, see: Lu, Y.; Nakano, M.; Ikeda, T. *Nature* **2003**, *425*, 145.
(6) (a) Ikeda, T.; Kanazawa, A. In *Molecular Switches*; Feringa, B. L., Ed.; Wiley-VCH: Weinheim, 2001; Chapter 12. (b) Boss, M. L.; Aramendia, P. F. *Photochem. Photobiol. Sci.* **2002**, *1*, 507. (c) Langhoff, A.; Giesselmann, F. *ChemPhysChem* **2002**, *3*, 424.
(7) (a) Pieroni, O.; Fissi, A.; Angelini, N.; Lenci, F. *Acc. Chem. Res.* **2001**, *34*, 9. (b) Willner, I.; Willner, B. In *Molecular Switches*; Feringa, B. L., Ed.; Wiley-VCH: Weinheim, 2001; Chapter 6. (c) Ciardelli, F.; Pieroni, O. In *Molecular Switches*; Feringa, B. L., Ed.; Wiley-VCH: Weinheim, 2001; Chapter 13.
(8) (a) Walter, D. G.; Campbell, D. J.; Mirkin, C. A. *J. Phys. Chem. B* **1999**, *103*, 402. (b) Janshoff, A.; Neitzert, M.; Oberdorfer, Y.; Fuchs, H. *Angew. Chem., Int. Ed.* **2000**, *39*, 3212. (c) Sortino, S.; Petralia, S.; Conoci, S.; Di Bella, S. *J. Mater. Chem.* **2004**, *14*, 811.

10.1021/ja0668466 CCC: $37.00

Scheme 1. Synthetic Scheme for (1-Cyclohexenyl)phenyldiazine (CPD) and Its Derivatives

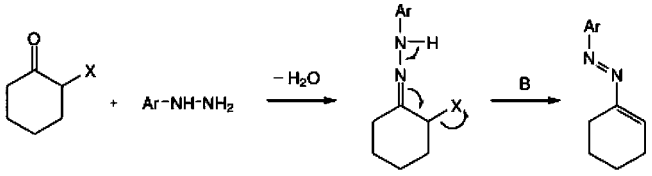

of more powerful (time-resolved) spectroscopic and computational techniques, the photoisomerization of azobenzene has been the subject of further detailed investigations with experimental[17] and theoretical[17f,18] approaches.

While it is well-known[1,2] that the photochemical behavior of azobenzene derivatives is strongly influenced by the substituents on the phenyl rings, not much information is available on the photoreactivity of azobenzene-type compounds in which the structure of the rings is changed. In particular, we are interested to see if and how the spectroscopic and photochemical properties change when the π-electron system adjacent to the $-N{=}N-$ double bond is reduced in size and the aromaticity has been eventually removed in one of the two rings. For this reason, we have synthesized and studied (1-cyclohexenyl)phenyldiazene (CPD, Chart 1), a species formally derived from azobenzene in which one of the phenyl rings is replaced by a cyclohex-1-ene moiety. Besides representing an azobenzene-type compound with reduced π-conjugation and aromaticity, its appeal resides also in its new funtionalization potentialities as revealed by its synthetic protocol (Scheme 1) that allows the preparation of arylazoalkenes with different ring sizes, too, which are prevented in the parent compound azobenzene and could be exploited for later applications.

Arylazoalkenes can be efficiently prepared from carbonyl derivatives bearing a good leaving group X on the carbon atom adjacent to the carbonyl function. The addition of arylhydrazine gives the corresponding arylhydrazone, a labile intermediate, that affords arylazoalkene by treatment with a mild base that promotes a clean 1,4-elimination of HX.[19] Typical reactions of arylazoalkenes are: (i) the conjugate addition of nucleophiles[19a,20] to the azo−ene moiety and (ii) the 4 + 2 cycloaddition reactions with a variety of carbon−carbon dienophiles and heterodienofiles, leading to the formation of six-membered heterocyclic compounds.[21]

Here, we report the results of an investigation on the photophysical and photochemical properties of CPD, carried out by electronic spectroscopic measurements and photochemical experiments in solution and by computational methods. In particular, fully unconstrained CASPT2//CASSCF/6-31G* minimum energy path computations have been used to elucidate the multistate dynamics and reaction coordinates, unveiling CPD's photochemical reactivity, as well as the energetics involved, and have achieved a full rationale of its photochemical behavior. For this purpose, the ground- and excited-state properties of CPD in the singlet manifold as well as in the triplet T_1 state, with specific reference to its $E \leftrightarrows Z$ isomerization reactions, are discussed in comparison to those of azobenzene.

2. Experimental and Computational Details

2.1. Experimental Section. Reagents and dry solvents were purchased from Fluka, unless otherwise noted. *E*-Azobenzene was purchased from Aldrich.

The absorption and luminescence spectra were recorded with a Varian Cary 50 spectrophotometer and a LS 50 spectrofluorimeter, respectively, on air-equilibrated acetonitrile or cyclohexane (Merck Uvasol) solutions at room temperature, with concentrations ranging from 1×10^{-5} to 1×10^{-4} M, contained in 1-cm quartz cells. Experimental errors: wavelengths, ± 1 nm; molar absorption coefficients, $\pm 5\%$.

Photochemical reactions were performed on the same solutions, thoroughly stirred, by using the Xe lamp (150 W) of a Perkin-Elmer 650-10S spectrofluorimeter. The monochromator of the instrument (bandpass = 10 nm) was employed for the selection of the desired irradiation wavelength. The number of incident photons, determined by ferrioxalate actinometry[22] in its micro version,[23] was between 10^{-8} and 10^{-7} *Nhν*/min. The $E \rightarrow Z$ quantum yields for $\pi\pi^*$ ($\lambda_{irr} = 325$ nm for CPD and 345 nm for AB; wavelengths of maximum conversion to the *Z* isomer) and $n\pi^*$ ($\lambda_{irr} = 430$ nm) irradiation were determined from the disappearance of the $\pi\pi^*$ absorption band of the reactant at low conversion percentages (<10%; if necessary, extrapolation to $t =$

(9) For representative examples, see: (a) Archut, A.; Vögtle, F.; De Cola, L.; Azzellini, G. C.; Balzani, V.; Ramanujam, P. S.; Berg, R. H. *Chem. Eur. J.* **1998**, *4*, 699. (b) Junge, D. M.; McGrath, D. V. *J. Am. Chem. Soc.* **1999**, *121*, 4912. (c) Sebastian, R. M.; Blais, J. C.; Caminade, A. M.; Majoral, J.-P. *Chem. Eur. J.* **2002**, *8*, 2172. (d) Uda, M.; Momotake, A.; Arai, T. *Photochem. Photobiol. Sci.* **2003**, *2*, 845. (e) Nithyanandhan, J.; Jayaraman, N.; Davis, R.; Das, S. *Chem. Eur. J.* **2004**, *10*, 689.

(10) (a) Balzani, V.; Scandola, F. *Supramolecular Photochemistry*; Horwood: Chichester, 1991; Chapter 7. (b) Shinkai, S. In *Molecular Switches*; Feringa, B. L., Ed.; Wiley-VCH: Weinheim, 2001; Chapter 9.

(11) For early, representative examples, see: (a) Ueno, A.; Yoshimura, H.; Saka, R.; Osa, T. *J. Am. Chem. Soc.* **1979**, *101*, 2779. (b) Shinkai, S.; Nakaji, T.; Nishida, Y.; Ogawa, T.; Manabe, O. *J. Am. Chem. Soc.* **1980**, *102*, 5860.

(12) Representative examples: (a) Shinkai, S.; Manabe, O. *Top. Curr. Chem.* **1984**, *121*, 67. (b) Ritter, G.; Häfelinger, G.; Lüddecke, E.; Rau, H. *J. Am. Chem. Soc.* **1989**, *111*, 4627. (c) Tamaoki, N.; Koseki, K.; Yamaoka, T. *Angew. Chem., Int. Ed. Engl.* **1990**, *29*, 105. (d) Vögtle, F.; Müller, W. M.; Müller, U.; Bauer, M.; Rissanen, K. *Angew. Chem., Int. Ed. Engl.* **1993**, *32*, 1295. (e) Röttger, O.; Rau, H. *Mol. Cryst. Liq. Cryst. Sci. Technol., Sect. A* **1994**, *246*, 143. (f) Bencini, A.; Bernardo, M. A.; Bianchi, A.; Ciampolini, M.; Fusi, V.; Nardi, N.; Parola, A. J.; Pina, F.; Valtancoli, B. *J. Chem. Soc., Perkin Trans. 2* **1998**, 413. (g) Cisnetti, F.; Ballardini, R.; Credi, A.; Gandolfi, M. T.; Masiero, S.; Negri, F.; Pieraccini, S.; Spada, G. P. *Chem. Eur. J.* **2004**, *10*, 2011.

(13) Kawata, S.; Kawata, Y. *Chem. Rev.* **2000**, *100*, 1777.

(14) (a) Qu, D.-H.; Wang, Q.-C.; Tian, H. *Angew. Chem., Int. Ed.* **2005**, *44*, 5296. (b) Qu, D.-H.; Wang, Q.-C.; Ma, X.; Tian, H. *Chem. Eur. J.* **2005**, *11*, 5929.

(15) Balzani, V.; Credi, A.; Venturi, M. *Molecular Devices and Machines: A Journey Into the Nano World*; Wiley-VCH: Weinheim, 2003.

(16) For recent examples of optomechanical devices based on azobenzene, see ref 14 and: (a) Hugel, T.; Holland, N. B.; Cattani, A.; Moroder, L.; Seitz, M.; and Gaub, H. E. *Science* **2002**, *296*, 1103. (b) Ji, H.-F.; Feng, Y.; Xu, X.; Purushotham, V.; Thundat, T.; Brown, G. M. *Chem. Commun.* **2004**, 2532. (c) Wang, Q.-C.; Qu, D.-H.; Ren, J.; Chen, K.; Tian, H. *Angew. Chem., Int. Ed.* **2004**, *43*, 2661. (d) Muraoka, T.; Kinbara, K.; Aida, T. *Nature* **2006**, *440*, 512.

(17) (a) Rau, H.; Luddecke, E. *J. Am. Chem. Soc.* **1982**, *104*, 1620. (b) Fujino, T.; Tahara, T. *J. Phys. Chem. A* **2000**, *104*, 4203. (c) Fujino, T.; Arzhantsev, S. Y.; Tahara, T. *J. Phys. Chem. A* **2001**, *105*, 8123. (d) Fujino, T.; Arzhantsev, S. Y.; Tahara, T. *Bull. Chem. Soc. Jpn.* **2002**, *75*, 1031. (e) Hirose, Y.; Yui, H.; Sawada, T. *J. Phys. Chem. A* **2002**, *106*, 3067. (f) Schultz, T.; Quenneville, J.; Levine, B.; Toniolo, A.; Martinez, T. J.; Lochbrunner, S.; Schmitt, M.; Shaffer, J. P.; Zgierski, M. Z.; Stolow, A. *J. Am. Chem. Soc.* **2003**, *125*, 8098. (g) Satzger, H.; Root, C.; Braun, M. *J. Phys. Chem. A* **2004**, *108*, 6265. (h) Chang, C.-W.; Lu, Y.-C.; Wang, T.-T.; Diau, E. W.-G. *J. Am. Chem. Soc.* **2004**, *126*, 10109. (i) Lu, Y.-C.; Diau, E. W.-G.; Rau, H. *J. Phys. Chem. A* **2005**, *109*, 2090.

(18) (a) Cattaneo, P.; Persico, M. *Phys. Chem. Chem. Phys.* **1999**, *1*, 4739. (b) Ishikawa, T.; Noro, T.; Shoda, T. *J. Chem. Phys.* **2001**, *115*, 7503. (c) Gagliardi, L.; Orlandi, G.; Bernardi, F.; Cembran, A.; Garavelli, M. *Theor. Chem. Acc.* **2004**, *111*, 363. (d) Diau, E. W.-G. *J. Phys. Chem. A* **2004**, *108*, 950. (e) Cembran, A.; Bernardi, F.; Garavelli, M.; Gagliardi, L.; Orlandi, G. *J. Am. Chem. Soc.* **2004**, *126*, 3234. (f) Ciminelli, C.; Granucci, G.; Persico, M. *Chem. Eur. J.* **2004**, *10*, 2327. (g) Tiago, M. L.; Ismail-Beigi, S.; Louie, S. G. *J. Chem. Phys.* **2005**, *122*, 94311. (h) Ciminelli, C.; Granucci, G.; Persico, M. *J. Chem. Phys.* **2005**, *123*, 174317.

(19) (a) Caglioti, L.; Rosini, G.; Rossi, F. *J. Am. Chem. Soc.* **1966**, *88*, 3865. (b) Hassner, A.; Catsoulacos, P. *J. Chem. Soc., Chem. Commun.* **1967**, 121. (c) Broda, S.; Simon, H. *Chem. Ber.* **1969**, *102*, 3647. (d) Buckingham, J.; Guthrie, R. D. *J. Chem. Soc.* (C) **1968**, 3079.

(20) Attanasi, O. A.; Filippone, P. *Synlett* **1997**, 1128 and references cited therein.

(21) Bonini, B. F.; Maccagnani, G.; Mazzanti, G.; Rosini, G.; Foresti, E. *J. Chem. Soc., Perkin Trans. I* **1981**, 2322 and references therein.

(22) Hatchard, C. G.; Parker, C. A. *Proc. R. Soc. London A* **1956**, *253*, 518.

(23) Fischer, E. *EPA Newsletter* **1984**, *20*, 33.

0 was made). The yields were calculated by taking into account the light absorbed by the sample at the irradiation wavelength. The composition of the photostationary state in the $E \rightarrow Z$ photoisomerization reactions was obtained by HPLC analysis; the absorption spectrum of the photoproduct (Z isomer) was evaluated by subtraction of the spectrum of the residual E isomer from the absorption spectrum at the photostationary state. The $Z \rightarrow E$ photoisomerization experiments were carried out with samples obtained by exhaustive irradiation of solutions of E-CPD at 325 nm and containing at least 80% of the Z isomer. The $Z \rightarrow E$ photoisomerization quantum yields were estimated[3] from the composition of the photostationary state by using eq 1:

$$\frac{\Phi_{E\rightarrow Z}}{\Phi_{Z\rightarrow E}} = \frac{\epsilon_Z^{\lambda_{irr}}}{\epsilon_E^{\lambda_{irr}}} \frac{[Z]_{PS}}{[E]_{PS}} \quad (1)$$

At room temperature and in the time scale of the irradiation experiments, the effect of the thermal $Z \rightarrow E$ isomerization—which is not taken into account in eq 1—can be safely neglected. The values of $\Phi_{E\rightarrow Z}$ and the molar absorption coefficients of the two isomers at the irradiation wavelength, $\epsilon_E^{\lambda_{irr}}$ and $\epsilon_Z^{\lambda_{irr}}$, were determined experimentally; d is the optical path length of the cell (1 cm). In the present system, the concentration of the E and Z species in solution can be calculated from the absorbance values monitored at two different wavelengths, λ_1 and λ_2:

$$[E] = \frac{A^{\lambda_1}\epsilon_Z^{\lambda_2} - A^{\lambda_2}\epsilon_Z^{\lambda_1}}{\epsilon_E^{\lambda_1}\epsilon_Z^{\lambda_2} - \epsilon_E^{\lambda_2}\epsilon_Z^{\lambda_1}} \quad (2)$$

$$[Z] = \frac{A^{\lambda_2}\epsilon_E^{\lambda_1} - A^{\lambda_1}\epsilon_E^{\lambda_2}}{\epsilon_E^{\lambda_1}\epsilon_Z^{\lambda_2} - \epsilon_E^{\lambda_2}\epsilon_Z^{\lambda_1}} \quad (3)$$

The concentrations of the two isomers at the photostationary state, $[E]_{PS}$ and $[Z]_{PS}$, were thus determined from eqs 2 and 3 for a solution at the photostationary state. Experimental error on the $E \rightarrow Z$ quantum yield values: ±10% for $\pi\pi^*$ irradiation, ±20% for $n\pi^*$ irradiation. For the $Z \rightarrow E$ photoisomerization quantum yields the error was estimated to be ±30%.

Photochemical experiments with the use of triplet sensitizers were carried out on solutions degassed by four freeze−pump−thaw cycles. On the basis of the triplet energies obtained by calculations (see below), biacetyl ($E_T = 56.4$ kcal mol^{-1})[24] was employed as photosensitizer for the T_1 excited state of E-CPD. The concentration of E-CPD was 5.0×10^{-5} M, and that of the photosensitizer was 2×10^{-2} M.

The thermally activated $Z \rightarrow E$ isomerization was studied by monitoring the absorption spectral changes in time for 5.0×10^{-5} M solutions previously subjected to exhaustive irradiation at 325 nm and containing at least 70% of the Z isomer. The temperature of the solution was controlled in the range 20−50 °C by means of a thermostat, and measured in the spectrophotometric cell by using a digital thermometer with a probe. The concentration values of the E isomer at various times were calculated by means of eq 2, and fitted according to a first-order rate equation by means of the SPECFIT software.[25] The E_a and A activation parameters were calculated with the Arrhenius relation, $k = A \exp(-E_a/RT)$. The values of ΔG^*, ΔH^*, and ΔS^* were calculated with the Eyring equation, $k = k_B T/h[\exp(-\Delta H^*/RT)][\exp(\Delta S^*/R)]$, and from $\Delta G^* = \Delta H^* - T\Delta S^*$. The error on the activation parameters was estimated to be ±5%.

2.2. Computational Section. The PES for the $E \leftrightarrows Z$ thermal- and photoisomerization have been studied using fully unconstrained optimizations and MEP computations at the CASSCF level[26] (when possible, single-state computations have been used; otherwise, when root-flipping problems occurred, state averaged calculations have been the choice), followed by single-point CASPT2[27] computations on the optimized relevant structures to account for correlation energy.

For this purpose a state-averaged CASSCF procedure, with equal weights between the involved states of the singlet manifold (the first seven singlet states in E-CPD and the first 10 singlet states in Z-CPD), has been used to generate molecular orbitals and the reference functions for subsequent CASPT2 calculations. An "Imaginary Shift"[28] value of 0.2 was employed for all state-averaged CASPT2 computations. This option is used to eliminate intruder states problems. For the triplet state, CASSCF single-state computations have been used in all cases, both for the optimizations and CASPT2 calculations. The CASSCF state interaction (CASSI)[29] method has been used to calculate the transition dipole moments. In the formula for the oscillator strength the CASSCF transition moment and the energy difference obtained in the CASPT2 computation have been used. All computations have been performed with the tools available in the Gaussian 98[30] and the MOLCAS-5[31] quantum chemistry programs.

The active space choice is a crucial step in a CASSCF calculation. Here the choice is straightforward, including all the orbitals and electrons of the π system plus the two doubly occupied nitrogen lone pairs, resulting in an active space of 12 orbitals and 14 electrons. A 6-31G* basis set of atomic orbitals was used. To improve vertical excitation energies, computations in the FC region were also performed by using the multistate-CASPT2 approach.[32] Diffuse functions (using a 6-31G+* basis set) or a generally contracted basis set of atomic natural orbitals (ano-l with the contraction scheme 4s3p2d on C and N, and 3s2p on H)[31] were also used for this purpose.

The search of conical intersections was performed by using procedures developed in our laboratory or according to the prescriptions of ref 33.

Four possible conformers exist for CPD. Two for the Z form: one with the cyclohexene C=C double bond and the N=N double bond in *s-trans* position (***Z*-MinS$_0$**), the other one with the two double bonds in *s-cis* position (***Z*-MinS$_0$′**). Analogously, there are two E isomer conformers: ***E*-MinS$_0$** and ***E*-MinS$_0$′**. Through a preliminary CASPT2//CASSCF calculation (see Table 5), we established that the most stable conformer is the ***E*-MinS$_0$** one. All successive mechanism calculations are relative to ***E*-MinS$_0$** for the E form isomerization and the corresponding photoproduct ***Z*-MinS$_0$** for the Z form.

3. Results and Discussion

3.1. Synthesis. (1-Cyclohexenyl)phenyldiazene (CPD). CPD has been prepared according to a well-established procedure. Phenylhydrazine (2.16 g, 20 mmol) was added at room temperature to a stirred solution of 2-bromocyclohexanone (3.52 g, 20 mmol) in toluene (100 mL). After 15 min the orange solution was washed first with 10% aqueous solution Na_2CO_3 and then with water, dried (Na_2SO_4), and concentrated under reduced pressure. The residue was purified by flash chromatography on a silica gel column eluting with toluene. A low-melting red-orange solid was collected: mp 32−34 °C from

(24) Montalti, M., Credi, A., Prodi, L., Gandolfi, M. T., Eds. *Handbook of Photochemistry*, 3rd ed.; CRC Press: Boca Raton, FL, 2006.
(25) Binstead, R. A. *SPECFIT*; Spectrum Software Associates: Chapel Hill, NC, 1996.
(26) Roos, B.O. In *Advances in Chemistry and Physics: Ab Initio Methods in Quantum Chemistry - II*; Lawley, K. P., Ed.; John Wiley & Sons Ltd.: Chichester, England, 1987; Vol. LXIX, p 399.
(27) Malmqvist, P.-Å.; Roos, B. O. *Chem. Phys. Lett.* **1989**, *155*, 189.
(28) Forsberg, N.; Malmqvist, P.-Å. *Chem. Phys. Lett.* **1997**, *274*, 196.
(29) Malmqvist, P.-Å.; Roos, B. O. *Chem. Phys. Lett.* **1989**, *155*, 189.
(30) Frisch, M. J.; et al. *Gaussian 98*, revision A.6; Gaussian, Inc.: Pittsburgh, PA, 1998.
(31) Andersson, K.; et al. *MOLCAS*, Version 5.2; Lund University: Lund, 2001.
(32) Finley, J.; Malmqvist, P.-Å.; Ross, B. O.; Searrano-Andres, L. *Chem. Phys. Lett.* **1998**, *288*, 299.
(33) (a) Ragazos, I. N.; Robb, M. A.; Bernardi, F.; Olivucci, M. *Chem. Phys. Lett.* **1992**, *197*, 217. (b) Bearpark, M. J.; Robb, M. A.; Schlegel, H. B. *Chem. Phys. Lett.* **1994**, *223*, 269.

Table 1. Absorption Data (Acetonitrile Solution, Room Temperature)

		$S_2 \leftarrow S_0$ ($\pi\pi^*$)		$S_1 \leftarrow S_0$ ($n\pi^*$)	
compound	isomer	λ_{max} (nm)	ϵ (M^{-1} cm^{-1})	λ_{max} (nm)	ϵ (M^{-1} cm^{-1})
CPD	*E*	304	22000	430	350
	Z	274	5100	429	1200
AB	*E*	316	21000	445	550
	Z	279	4300	428	1200

methanol;[19c] bp 110−120 °C (0.05 mmHg). Spectroscopic and analytical data agree with those previously reported.[34]

3.2. Absorption Spectra: The Singlet Manifold.

Experiments. The spectroscopic data for CPD and AB, obtained at room temperature in acetonitrile solution, are gathered in Table 1. The absorption spectrum of the *E* isomer of CPD is shown in Figure 1 together with the spectrum of *E*-AB. The absorption spectrum of *E*-CPD is qualitatively similar to that of *E*-AB, and exhibits two bands in the 250−520 nm region. In analogy with azobenzene, the low-energy band of *E*-CPD is attributed to $S_1 \leftarrow S_0$ ($n\pi^*$) transitions, and the higher-energy band is assigned to $S_2 \leftarrow S_0$ ($\pi\pi^*$) transitions. Both absorption bands, however, are noticeably shifted to higher energy on going from *E*-AB to *E*-CPD (~800 and ~1200 cm^{-1} for the $n\pi^*$ and $\pi\pi^*$ bands, respectively). This observation is not unexpected, considering the reduced size of the π-electron system in CPD with respect to AB. The molar absorption coefficient of the $S_2 \leftarrow S_0$ band is nearly the same as that of azobenzene, while in the case of the $S_0 \leftarrow S_1$ band the molar absorption coefficient of *E*-CPD is somewhat smaller than that of *E*-azobenzene.

The absorption spectrum of the *Z* isomer of CPD is almost identical to that of *Z*-AB (Table 1 and Figure 2) and exhibits a two-band pattern with well separated $n\pi^*$ and $\pi\pi^*$ absorption features. The only noticeable difference between the two spectra is a modest (~700 cm^{-1}) shift of the $S_2 \leftarrow S_0$ band of *Z*-CPD to higher energy, compared to the same band in *Z*-AB, and a slightly larger intensity. The shift can again be interpreted in terms of a larger extension of the π-electron system in azobenzene.

The spectral features of both isomers of CPD and AB do not change appreciably on going from acetonitrile to a less polar solvent like cyclohexane. *E*- and *Z*-CPD do not exhibit fluorescence either in fluid solution at room temperature or in a frozen glass at 77 K, in line with the behavior of azobenzene.[1,2,35]

Calculations. CASPT2//CASSCF/6-31G* vertical transitions and oscillator strengths (***f***) have been computed in vacuo for the first low-energy states of the singlet manifold (the first 7 singlet states in *E*-CPD and the first 10 singlet states in *Z*-CPD), as reported in Tables 2 (***E*-MinS$_0$**) and 3 (***Z*-MinS$_0$**). It turns out that the computed $S_1 \leftarrow S_0$ ($n\pi^*$) transitions slightly underestimate the experimentally detected excitation energies in solution (i.e., the low-energy band of the absorption spectra)

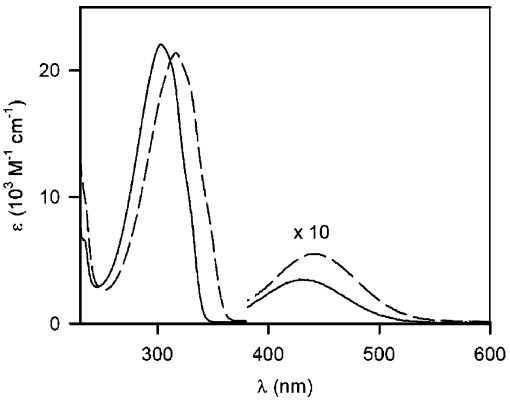

Figure 1. Absorption spectra in acetonitrile solution at room temperature of the *E* isomers of CPD (full line) and AB (dashed line).

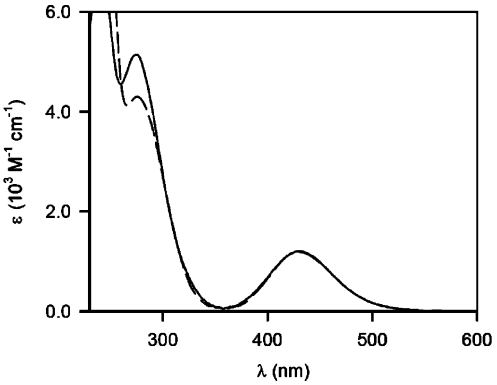

Figure 2. Absorption spectra in acetonitrile solution at room temperature of the *Z* isomers of CPD (full line) and AB (dashed line).

by 6.6 and 2.8 kcal/mol respectively for *E*-CPD and *Z*-CPD (as compared with the data in Table 1). Computed oscillator strengths (~10^{-5} for *E*-CPD and ~10^{-2} for *Z*-CPD) are consistent with a forbidden $n\pi^*$ excitation in *E*-CPD ($\epsilon = 350$ M^{-1} cm^{-1}), but a more intense (i.e., slightly allowed) transition in *Z*-CPD ($\epsilon = 1200$ M^{-1} cm^{-1}). While these data are acceptable and in fairly good agreement with the experiments, more serious problems arise in reproducing excitation energies for the bright $S_2 \leftarrow S_0$ ($\pi\pi^*$) transitions (i.e., the higher-energy band of the absorption spectra). Our computations overestimate these energies by 19.2 kcal/mol—assigning this state as S_3 (S_5 at the CASSCF level)—and 16.3 kcal/mol—assigning this state as S_5 (S_9 at the CASSCF level)—for *E*-CPD and *Z*-CPD, respectively, while the computed oscillator strengths (0.3 for *E*-CPD and 0.1 for *Z*-CPD) are roughly in line with the measured molar absorption coefficients of a spectroscopically allowed transition (22000 M^{-1} cm^{-1} for *E*-CPD and 5100 M^{-1} cm^{-1} for *Z*-CPD). These errors can be only slightly reduced by adding diffuse functions to the basis set (6-31G+*), while $n\pi^*$ transitions remain substantially unchanged (see Supporting Information). Interestingly, if we correct these energies to match experimental values, we can see that the bright $\pi\pi^*$ state become S_2 in both cases, with nearby (i.e., nearly degenerate) $\pi_{benz}\pi^*$ states involving benzenic excitations, as already known for AB. We confidently think this should be the correct energy order in the singlet manifold.

While the computed energies for the bright $\pi\pi^*$ excitation are far from being satisfactory, we will see below that these errors do not affect at all our Discussion and Conclusions on the reactivity and photochemical/photophysical properties of

(34) Caglioti, L.; Grasselli, P.; Rosini, G. *Tetrahedron Lett.* **1965**, 4545.
(35) A very weak fluorescence band ($\Phi_{fl} \approx 10^{-6}$), displaying an ultrafast (subpicosecond) decay, has been recently observed for AB at room temperature in DMSO (see: Satzger, H.; Sporlein, S.; Root, C.; Wachtveitl, J.; Zinth, W.; Gilch, P. *Chem. Phys. Lett.* **2003**, *372*, 216) and hexane solution (see: Fujino, T.; Arzhantsev, S. Y.; Tahara, T. *J. Phys. Chem. A* **2001**, *105*, 8123). Such an emission band, if present for CPD, has an intensity below the detection limit of our instrumentation ($\Phi_{fl} < 10^{-5}$).

Table 2. CASPT2 and CASSCF Relative (ΔE) Energies and $S_n \leftarrow S_0$ Oscillator Strengths (*f*) for All the Relevant Points Discussed in the Text along the Photochemical Paths of the *E* Isomer[a]

		CASPT2		CASSCF				CASPT2	CASSCF
structure	state	ω	ΔE (kcal mol^{-1}) *[nm]*	ΔE (kcal mol^{-1}) *[nm]*	*f*	structure	state	ω	ΔE (kcal mol^{-1})	ΔE (kcal mol^{-1})
***E*-MinS$_0$**	S_0	.64	0.0	0.0		***E*-MinS$_1$**	S_0	.64	18.4	17.4
	S_1	.63	59.9 *[477]*	74.6 *[383]*	~0		S_1	.63	46.4	58.7
	S_2	.63	99.0 *[289]*	108.1 *[264]*	0.004		S_2	.63	95.5	113.3
	S_3	.62	112.9 *[253]*	150.0 *[190]*	0.325	***E*-TS$_{S1}$**	S_0	.64	28.5	31.9
	S_4	.63	115.0 *[249]*	133.7 *[214]*	0.005		S_1	.63	49.2	63.0
	S_5	.63	119.1 *[240]*	133.3 *[214]*	0.008		S_2	.63	81.0	93.6
	S_6	.62	126.8 *[225]*	150.4 *[190]*	0.0185	***E*-CI$_{tors1}$** [b]	S_0	.63	45.7	55.5
							S_1	.64	53.5	61.1
						***E*-CI$_{tors2}$** [b]	S_0	.63	31.6	52.4
							S_1	.63	36.1	58.1
						MIN−T$_{S2}$	S_0	.63	39.3	47.3
							S_1	.63	50.5	67.4
							S_2	.63	60.8	78.6
						***E*-TS$_{S2}$**	S_1	.63	68.0	88.8
							S_2	.63	91.9	98.6
							S_3	.63	98.6	109.6
						***E*-MinS$_2$**	S_2	.63	89.5	98.6
							S_3	.63	105.4	113.5
						***E*-CI$_{d_inv}$** [b]	S_0	.63	63.9	75.6
							S_1	.64	76.5	76.7
						***E*-CI$_{inv1}$** [b]	S_0	.63	58.3	68.8
							S_1	.64	64.6	73.7
						***E*-CI$_{inv2}$**	S_0	.63	66.8	78.7
							S_1	.63	67.3	76.5

[a] Singlet states (S_n) are ordered according to CASPT2 results. Energy values are state averaged through the first 7 singlet states. The energy for the ground state minimum is chosen as the zero. Basis set: 6-31G*. Active space: 14 electrons in 12 MOs. The weight (ω) of the zeroth order CASSCF wave function has also been reported. [b] The nature of singlet sates is already exchanged: S_0 is an nπ* state, and S_1 has the ground-state configuration.

Table 3. CASPT2 and CASSCF Relative (ΔE) Energies and $S_n \leftarrow S_0$ Oscillator Strengths (*f*) for All the Relevant Points Discussed in the Text along the Photochemical Paths of the *Z* Isomer[a]

		CASPT2		CASSCF				CASPT2	CASSCF
structure	state	ω	ΔE (kcal mol^{-1}) *[nm]*	ΔE (kcal mol^{-1}) *[nm]*	*f*	structure	state	ω	ΔE (kcal mol^{-1})	ΔE (kcal mol^{-1})
***Z*-MinS$_0$**	S_0	.64	0.0	0.0		***Z*-CI$_{tors1}$** [b]	S_0	.63	30.2	36.4
	S_1	.63	63.8 *[448]*	77.5 *[369]*	0.008		S_1	.64	37.8	40.7
	S_2	.62	104.5 *[274]*	124.0 *[231]*	0.005	***Z*-CI$_{tors2}$** [b]	S_0	.63	29.2	34.2
	S_3	.63	105.9 *[270]*	112.7 *[254]*	0.0004		S_1	.64	33.9	38.7
	S_4	.62	117.0 *[244]*	139.0 *[206]*	0.003	***Z*-CI$_{S2/S1}$**	S_1	.63	59.3	79.7
	S_5	.60	120.6 *[237]*	178.0 *[161]*	0.108		S_2	.63	63.3	77.5
	S_6	.62	128.4 *[223]*	152.8 *[187]*	0.016	**INTs$_2$**	S_2	.63	77.3	89.8
	S_7	.62	133.9 *[214]*	162.2 *[176]*	0.002		S_3	.63	87.8	99.8
	S_8	.62	139.2 *[205]*	161.1 *[177]*	0.007		S_4	.62	100.1	117.8
	S_9	.62	141.6 *[202]*	166.7 *[172]*	0.001	***Z*-CI$_{inv1}$**	S_0	.64	59.0	62.7
							S_1	.63	67.4	71.1
						***Z*-CI$_{inv2}$** [b]	S_0	.63	56.6	62.2
							S_1	.63	57.9	67.6
						***Z*-CI$_{d_inv}$**	S_0	.63	60.2	67.6
							S_1	.63	64.0	70.1
						INTs$_1$	S_0	.64	2.5	2.7
							S_1	.63	58.7	72.6

[a] Singlet states (S_n) are ordered according to CASPT2 results. Energy values are state averaged through the first 10 singlet states. The energy for the ground-state minimum is chosen as the zero. Basis set: 6-31G*. Active space: 14 electrons in 12 MOs. The weight (ω) of the zeroth order CASSCF wave function has also been reported. [b] The nature of singlet sates is already exchanged: S_0 is an nπ* state, and S_1 has the ground-state configuration.

CPD. Anyway, in the attempt to improve these energies and correct such a surprising mismatch (which should not generally occur at such a correlated high level of theory), multistate-CASPT2 (MS-CASPT2) computations have also been performed in conjunction with a larger basis set (ano-l). Notably, the results lead to significantly improved excitation energies (97.9 kcal/mol and 112.9 kcal/mol for the bright $\pi\pi$* excitation of the *E* and *Z* isomers, respectively) in much better agreement with the experimental values (94.0 and 104.3 kcal/mol, see also Supporting Information for details). Anyway, this computational level has not been further used due to its computational cost.

3.3. *E* ⇆ *Z* Photochemical and Thermal Isomerization.

Direct Irradiation Experiments. The quantum yields for $E \rightarrow Z$ and $Z \rightarrow E$ photoisomerization at selected irradiation wavelengths in acetonitrile solution are reported in Table 4. As a control experiment the photoisomerization of azobenzene was also studied under our experimental conditions. The quantum yield values determined for AB are in agreement with those found in earlier accurate studies.[3]

The absorption changes observed upon irradiation of *E*-CPD in its $S_2 \leftarrow S_0$ ($\pi\pi$*) absorption band at 325 nm are shown in Figure 3. Such changes are fully consistent with the $E \rightarrow Z$

Table 4. Data for the $E \rightarrow Z$ and $Z \rightarrow E$ Photoisomerization Processes at Room Temperature and the $Z \rightarrow Z$ Isomerization Reaction (acetonitrile Solution)

	E–Z photoisomerization								
	$\Phi_{E\rightarrow Z}$		$\Phi_{E\rightarrow E}$		*Z* → *E* thermal isomerization				
compd	$\pi\pi^*$ [a]	$n\pi^*$ [b]	$\pi\pi^*$ [c]	$n\pi^*$ [b]	E_a (kcal mol^{-1})	A (s^{-1})	ΔH^* (kcal mol^{-1})	ΔS^* (cal K^{-1} mol^{-1})	ΔG^*_{298} (kcal mol^{-1})
CPD	0.17	0.30	0.3[c]	0.7[c]	22.5	8.2×10^{11}	21.9	−6.1	22.3
AB	0.14	0.31	0.35[d]	0.55[d]	23.9[e]	2.43×10^{11} [c]	23.2[f]	−8.6[f]	25.8[f]

[a] $\lambda_{irr} = 325$ nm for CPD and 345 nm for AB. [b] $\lambda_{irr} = 430$ nm. [c] Values calculated by eq 1. [d] From ref 36. [e] From ref 39a. [f] Calculated from the data reported in ref 39a: $\Delta H^* = E_a - RT$; $\Delta S^* = [(\ln A) - 1.00 - \ln(k_B T/h)]$; $\Delta G^*_{298} = \Delta H^* - 298\Delta S^*$.

isomerization of the −N═N− unit. Neat isosbestic point are observed at 261 and 365 nm, indicating the occurrence of a clean transformation. A photostationary state that contains ∼85% of the *Z*-CPD isomer is reached within 30 min of irradiation in our conditions. Irradiation in the $S_1 \leftarrow S_0$ ($n\pi^*$) absorption band at 430 nm causes the same spectral changes observed for 325-nm excitation; the photostationary state, however, is much less rich in the *Z* form (∼10%), mainly because of the unfavorable ratio of the molar absorption coefficients of the *E* and *Z* isomers (see Experimental Section).

Similarly to azobenzene, either $n\pi^*$ or $\pi\pi^*$ excitation of the *Z* isomer of CPD leads to its conversion back to the *E* isomer, as confirmed by absorption spectral changes opposite to those observed on irradiation of the *E* form. In all cases the photoisomerization quantum yield values are remarkably higher for $n\pi^*$ irradiation compared to those obtained on $\pi\pi^*$ irradiation (Table 4). This is again in line with the behavior of azobenzene (see Table 2).[1−3,36] Although CPD does substantially behave as AB, it is noteworthy that the former gives a much higher ($n\pi^*$) $\Phi_{Z\rightarrow E}$ quantum yield.

The photoreactivity of both isomers of CPD and AB do not change appreciably on going from acetonitrile to a less polar solvent such as cyclohexane.

Computational Analysis of the Photochemistry upon $n\pi^*$ Excitation. The results of CASPT2//CASSCF/6-31G* minimum energy path (MEP) mapping from the Franck−Condon (FC) region (i.e., the region initially populated by vertical excitation) of the S_1 ($n\pi^*$) state of the *E* and *Z* isomers of CPD are summarized in Figures 4 and 5 (blue arrows) respectively, while Tables 2 and 3 collect the relative energies of all the relevant points discussed (for absolute energy values see Tables S3 and S4 in the Supporting Information). The reaction paths, which appear to be analogous to the ones previously documented by us for the S_1 ($n\pi^*$) state of AB,[18e] clearly account for the existence in both isomers of efficient $S_1 \rightarrow S_0$ radiationless deactivations, which are triggered by easily accessible low-energy S_1/S_0 real crossing points (i.e., conical intersections) with a fully twisted (∼90°) central −N−N− bond (***E*-CI$_{tors2}$** and ***Z*-CI$_{tors1}$**), prompting the isomerization of the system upon decay to the ground state. Interestingly, as already pointed out in AB,[18e] a barrierless path exists for the *Z* isomer, which directly connects the FC region on S_1 to a twisted low-energy S_1/S_0 conical intersection (CI) point, while an extended energy plateau (with a very shallow planar minimum ***E*-MinS$_1$** and a tiny energy barrier at ∼50° of CNNC torsion, ***E*-TS$_{S1}$**) exists along the S_1 path of the *E* isomer.

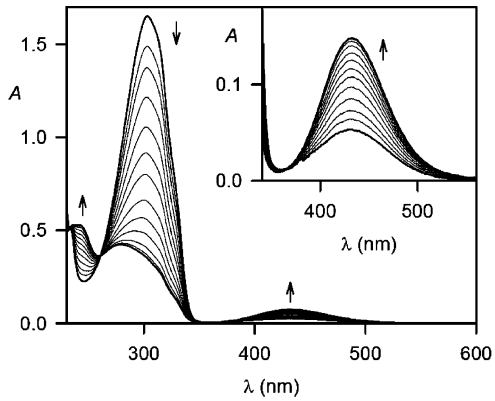

Figure 3. Absorption changes upon 325-nm irradiation of a 7.5×10^{-5} M acetonitrile solution of *E*-CPD at room temperature. Irradiation times are 0, 1, 2, 4, 6, 8, 10, 13, 16, 20, 25, 30, and 35 min. (Inset) Detail of the changes in the $S_1 \leftarrow S_0$ ($n\pi^*$) absorption band.

Interpretation of Photoisomerization Quantum Yields. These results clearly indicate that for both the *E* and *Z* isomers the S_1 state internal conversion involves mainly the torsion route, in agreement with the experiments and photoisomerization quantum yields measurements (Table 4). To determine quantitatively the $E \leftrightarrows Z$ isomerization quantum yields, a more complete characterization of the S_1 potential energy surface (PES) around these CIs and molecular dynamics simulations would be required. Nevertheless, at a qualitative level, the barrierless versus the barrier-controlled twisting path accounts for the observed higher yield (∼70%) of the $Z \rightarrow E$, with respect to the $E \rightarrow Z$ (30%), photoisomerization process. Moreover, the lowest-energy S_1/S_0 real crossing points found from both the *E* and *Z* form (which are basically the same structure), are placed slightly on the *E* side (i.e., the −N−N− twisting angle is around 93°), which accounts for a ground-state relaxation process leading preferentially to the *E* isomer formation. Note also that the sum of the $\Phi_{Z\rightarrow E}$ ($n\pi^*$) and $\Phi_{E\rightarrow Z}$ ($n\pi^*$) quantum yields equals one, which suggests a common deactivation point for both the *E* and *Z* forms as computations reveal.

Computational Analysis of the Photochemistry upon $\pi\pi^*$ Excitation. The results of CASPT2//CASSCF/6-31G* MEP mapping from the FC point of the first bright $\pi\pi^*$ singlet state of the *E* and *Z* isomers of CPD are summarized in Figures 4 and 5 (red arrows) respectively, while Tables 2 and 3 collect the relative energies of all the relevant points discussed (for absolute energy values see Tables S3 and S4 in the Supporting Information). As mentioned above, this state is overestimated in energy for both isomers. Anyway, as already seen in AB, both isomers display an unbound state (characterized by a double excitation), which is higher in energy in the FC point but suddenly crosses the $\pi\pi^*$ state along the MEP, getting lower in energy. Therefore, an ultrafast depopulation/deactivation of the bright state is expected in favor of this double-excitation

(36) Siampiringue, N.; Guyot, G.; Monti, S.; Bortolus, P. *J. Photochem.* **1987**, *37*, 185.

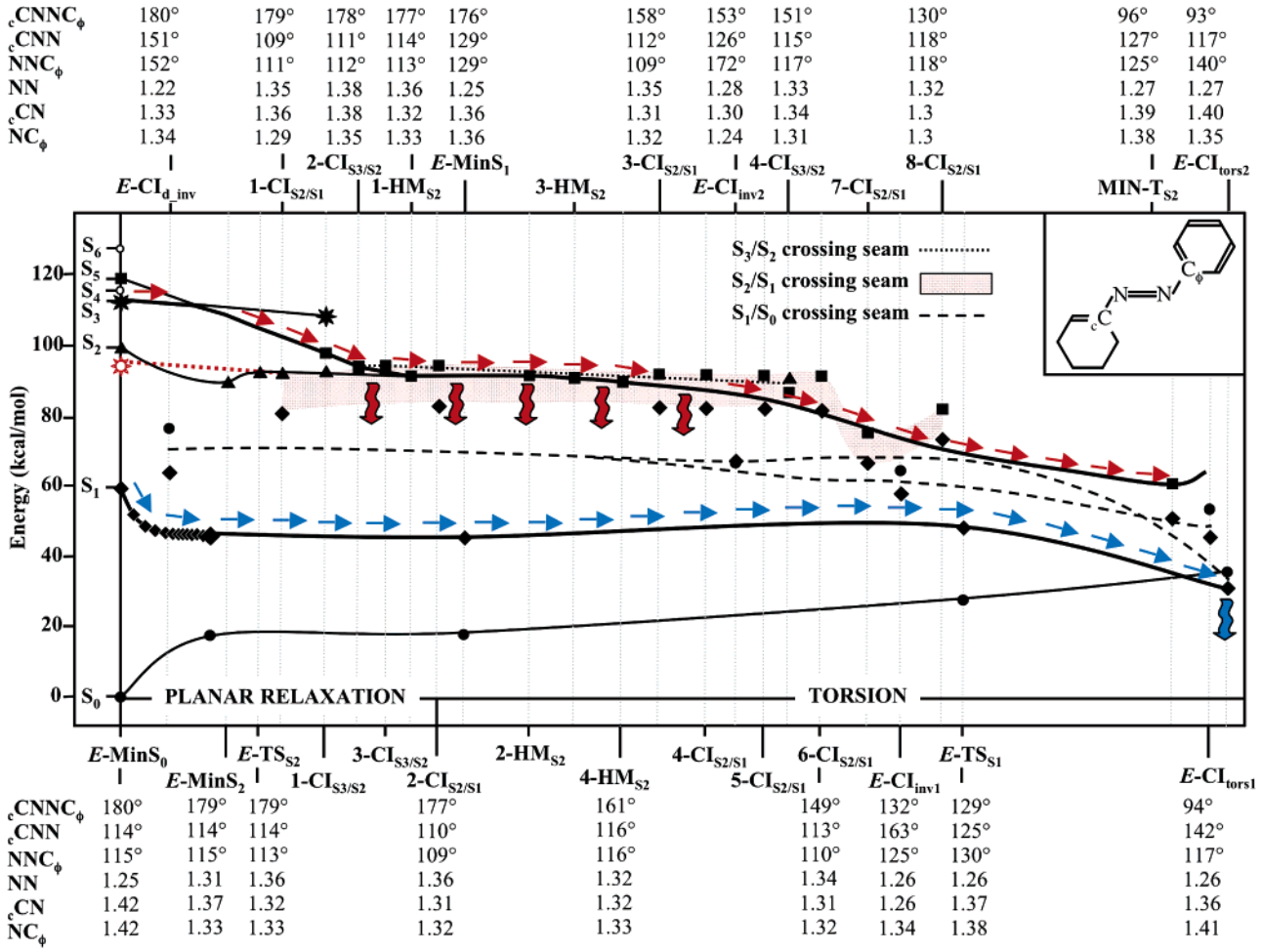

Figure 4. *E*-CPD computed reaction paths upon nπ^* and $\pi\pi^*$ excitations. Blue arrows show the nπ^* state (solid diamonds) MEP from the Franck−Condon region to the low-energy S_1/S_0 crossing point (−N=N− torsions are mainly involved); red arrows show the MEP from the bright $\pi\pi^*$ state (solid asterisks). The higher double-excitation state (solid squares) suddenly crosses the $\pi\pi^*$ state and drives the relaxation of the excited molecule. The dotted red points zone represents the extended S_2/S_1 crossing seam. The red dotted line is the bright $\pi\pi^*$ state scaled to match the experimental absorption value. All the energy profiles have been scaled to match CASPT2 values (Table 2).

$(n\pi^*)^2$ state, which thereafter drives the relaxation of the excited molecules.[37]

Interestingly, initial relaxation from the $\pi\pi^*$ FC point of the *Z* isomer does suddenly involve the −N−N− bond torsion leading (through a barrierless and steep path) to a partially twisted (65°) $S_2(n\pi^*)^2/S_1(n\pi^*)$ surface crossing (**Z-CI$_{S2/S1}$**), which easily accounts for a rapid $S_2 \rightarrow S_1$ nonradiative decay. In contrast, −N−N− bond torsion is not initially involved in the $\pi\pi^*$ relaxation of the *E* isomer, which is characterized by a more general skeletal rearrangement leading to an increase in N−N bond length and a decrease in C−N bonds. Only after this skeletal rearrangement has occurred, torsion around the N−N bond starts, still spanning a flat and extended energy region before reaching the fully twisted (96°) minimum (**MIN**−T$_{S2}$) on the S_2 $(n\pi^*)^2$ state (see Figure 4 and Table S3 in the Supporting Information for the energies of the optimized points along the S_2 MEP, from **1-HM$_{S2}$** to **4-HM$_{S2}$**). Notably, a significant S_2/S_1 energy gap exists for *E* at this point, suggesting a different (and hopefully more efficient) radiationless decay route to S_1. Remarkably, an extended S_2/S_1 crossing region exists which is almost degenerate and parallel to the computed MEP on the S_2 state (see Figure 4 and Table S3 in the Supporting Information for the energies of the computed S_2/S_1 crossing points, from **1-CI$_{S2/S1}$** to **8-CI$_{S2/S1}$**). We have proved that this crossing seam can be easily accessed by moving orthogonally to the S_2 MEP along symmetric CNN bending modes (CNN bendings must get smaller to reach this crossing region; see the geometrical parameters reported in Figure 4) and that this motion is substantially barrierless. Furthermore, the extended and continuous S_2/S_1 crossing region, which runs parallel and isoenergetic to almost the whole S_2 MEP, grants a high probability for the excited molecules to enter this space by normal thermal vibrations (see Scheme 2). Hence, decay to the $S_1(n\pi^*)$ state at −N−N− twisting angles that are far from being fully twisted, must be very likely and efficient.

Exploration and Analysis of the S_1/S_0 Crossing Region. Once the $S_1(n\pi^*)$ state has been populated, this will drive deactivation to the ground state according to the accessibility of the S_1/S_0 crossing regions which trigger $S_1(n\pi^*) \rightarrow S_0$

(37) This mechanism should remain substantially unchanged even if we place the bright state at the experimentally correct energy level (see red dotted lines in Figures 4 and 5 for experimentally scaled energies); also in this case the double-excitation state, which gets lower in energy, is easily populated directly by crossing the $\pi\pi^*$ state or by mediation of an excited state of benzenic character ($\pi_{benz}\pi^*$), which is almost degenerate to the spectroscopic state. In conclusion, whatever be the specific case considered, excited-state relaxation from the bright $\pi\pi^*$ state should end up in its rapid deactivation to an unbound double-excited $(n\pi^*)^2$ state.

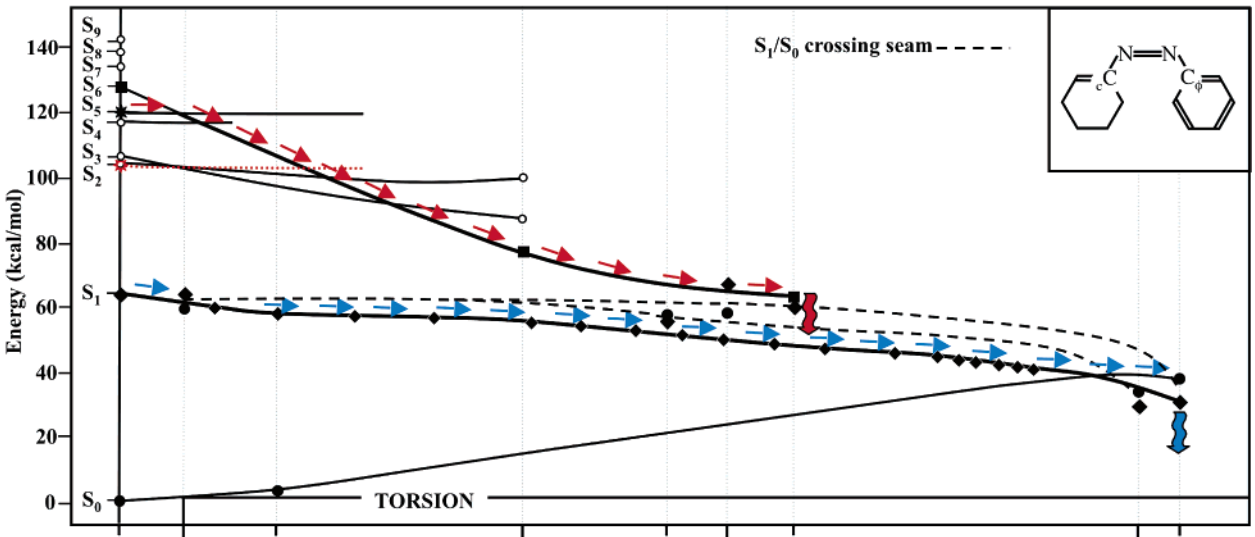

	Z-MinS$_0$	Z-CI$_{d_inv}$	INT$_{S1}$	INT$_{S2}$	Z-CI$_{inv2}$	Z-CI$_{inv1}$	Z-CI$_{S2/S1}$	Z-CI$_{tors1}$	Z-CI$_{tors2}$	
$_cCNNC_\phi$	4°	4°	13°	42°	51°	55°	65°	93°	94°	
$_cCNN$	122°	156°	125°	118°	126°	163°	119°	117°	142°	
NNC_ϕ	122°	155°	124°	124°	171°	139°	119°	140°	117°	
NN	1.24	1.21	1.26	1.33	1.27	1.26	1.36	1.27	1.26	
$_cCN$	1.44	1.28	1.41	1.42	1.28	1.40	1.32	1.39	1.36	
NC_ϕ	1.43	1.37	1.41	1.32	1.24	1.28	1.32	1.35	1.41	

Figure 5. Z-CPD reaction paths upon nπ^* and $\pi\pi^*$ excitation. Blue arrows show the nπ^* state (solid diamonds) MEP from the Franck−Condon region to the low-energy S_1/S_0 crossing point (−N=N− torsions are mainly involved); red arrows show the MEP from the bright $\pi\pi^*$ state (solid asterisks). The higher double excitation state (solid squares) suddenly crosses the $\pi\pi^*$ state and drives the relaxation of the excited molecule. The red dotted line is the bright $\pi\pi^*$ state scaled to match the experimental absorption value. All energy profiles have been scaled to match CASPT2 values (Table 3).

Scheme 2. Cartoonlike Drawing Showing the Extended S_2/S_1 Crossing Seam Running Almost Parallel to the Computed S_2 MEP[a]

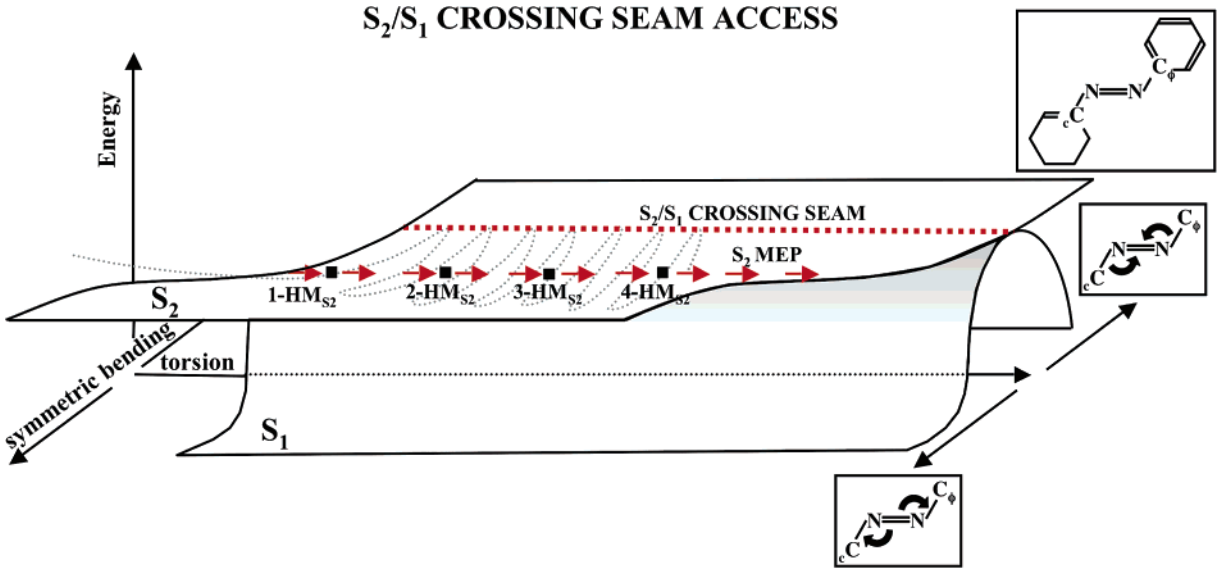

[a] The crossing seam can be accessed by vibrations (e.g., symmetric CNN bending modes) orthogonal to the MEP.

radiationless decay. For this reason, to access the feasibility of multiple deactivation channels, an extended investigation and analysis of the S_1/S_0 crossing seam has been performed, from low-energy to higher-energy conical intersection points. In particular, these former points may become accessible in a condition of excess vibrational energy, as it is when the molecule is decaying from the higher-energy $\pi\pi^*$ state.

A complex S_1/S_0 crossing subspace exists, with energies that all lie below the extended S_2/S_1 crossing region from which decay to S_1 occurs. The topology of this crossing space is substantially identical in the two isomers, and spans very different structures, going from the lowest-energy geometries with a fully twisted −N−N− bond (see ***E*-CI$_{tors1}$**, ***E*-CI$_{tors2}$**, ***Z*-CI$_{tors1}$**, and ***Z*-CI$_{tors2}$**), to higher-energy *inverted* (i.e., one of the CNN bending angles is linear, while the other is much smaller, thus calling for an *inversion* mechanism in the photoisomerization, see ***E*-CI$_{inv1}$**, ***E*-CI$_{inv2}$**, ***Z*-CI$_{inv1}$**, ***Z*-CI$_{inv2}$**) or *symmetric* (i.e., identical CNN bendings, see ***E*-CI$_{d_inv}$**, ***Z*-CI$_{d_inv}$**) structures. More precisely, the S_1/S_0 crossing seam, which is schematically depicted in Scheme 3, has a symmetric

Scheme 3. Cartoonlike Drawing Representing the Topology of the S_1/S_0 Crossing Region

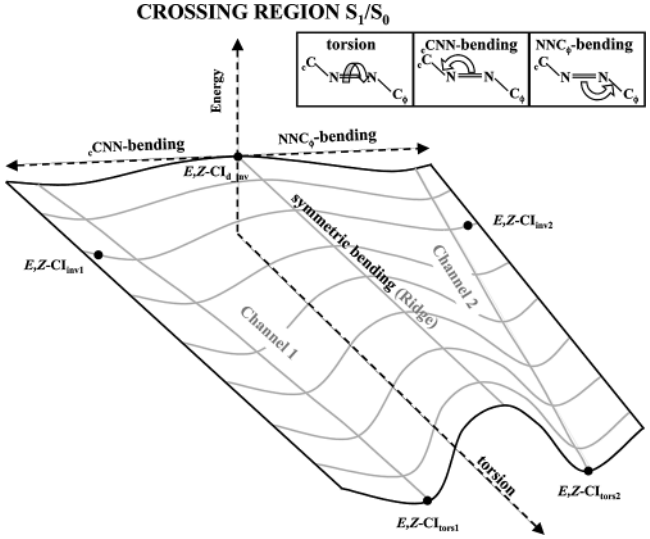

shape with a ridge of *symmetric* (i.e., identical CNN bendings) conical intersections separating a two-fold channel (one collecting conical intersections with a CNN bending angle that is larger than the other, such as ***Z,E*-CI$_{tors1}$** and ***Z,E*-CI$_{inv1}$**, and the other collecting the corresponding pseudo-enantiomeric structures, i.e., with CNN bending angles of inverted order such as ***Z,E*-CI$_{tors2}$** and ***Z,E*-CI$_{inv2}$**).[38] Remarkably, this crossing subspace is wholly connected, i.e., one can freely move from one conical intersection to the other without never exiting the intersection space (see Supporting Information for details). In general, identical bending angles (i.e., *symmetric* CIs) lead to the highest energies (i.e., the ridge), while a decrease in energy is observed when the symmetry is broken (i.e., different bending angles) and the CNNC angle gets more and more twisted.

In conclusion, the lowest-energy points in the S_1/S_0 crossing seam are the asymmetric CIs described in the previous section for nπ^* photochemistry, which possess a fully twisted −N−N− bond. These points are the only ones accessible for cold systems, i.e., in conditions of a small excess of vibrational energy, while very different S_1/S_0 CIs can be potentially entered on decaying from higher-energy regions, such as from the $\pi\pi^*$ state.

Interpretation of Photoisomerization Quantum Yields. At a qualitative level, the barrierless and steep S_2 relaxation path found for the *Z* isomer (which is dominated by the −N−N− torsional motion), versus the comparatively flat twisting path found for the *E* isomer, accounts for the observed higher yield (30%) of the $Z \rightarrow E$, with respect to the $E \rightarrow Z$ (17%), photoisomerization process. In fact, while along the first path decay to S_1 can occur around a CNNC twisting of 65° (i.e., the S_2/S_1 CI, see Figure 5) with an impulsive motion about this torsional mode (therefore providing the driving force triggering $Z \rightarrow E$ photoisomerization), $S_2 \rightarrow S_1$ decay for the *E* isomer can occur at much less twisted structures (see discussion above). Moreover, initial relaxation from the $\pi\pi^*$ FC region does not involve −N−N− torsions at all, and under these conditions no excess vibrational energy is expected to populate this mode in the short lifetime of S_2.

Another interesting point concerns the difference of photoisomerization quantum yields observed in the $\pi\pi^*$ and nπ^* states (i.e., the Kasha rule is violated), with the former invariably larger than the latter, as in AB. Since we have just shown that all the photoexcited molecules are ultimately collected in the S_1 nπ^* state (which then drives the deactivation onto the ground state), such an observation can appear somewhat surprising. This suggests that we are dealing with a dynamical problem, as recently shown by Persico and co-workers for AB.[18f] Therefore, to correctly account for this phenomenon, molecular dynamical simulations would be required which is beyond the scope of this work. Nevertheless, a qualitative (but reasonable) explanation may be drawn if we focus into the complex S_1/S_0 crossing region described above. As we have seen, $S_2 \rightarrow S_1$ decay occurs at energies that are invariably higher than the S_1/S_0 crossing region, with this subspace extending widely below the S_2/S_1 intersection space. It is likely that, following $S_2 \rightarrow S_1$ decay, molecules on the S_1 state may intercept the S_1/S_0 crossing region well above the lowest-energy −N−N− fully twisted CIs: for instance, at crossing points with CNNC angles which are only partially twisted, i.e., on the reactant side (as shown in Scheme 4). Actually, we may predict that such a situation is quite common and favorable, since this region extends for a wide portion below the S_2 state. This should trigger the population of ground-state relaxation channels leading preferentially to reactant back formation, which accounts for the smaller quantum yield observed from the $\pi\pi^*$ state.

***E* ⇆ *Z* Photoisomerization by Triplet Sensitization.** In order to explore the reactivity of the T_1 (nπ^*) triplet excited state, the $E \leftrightarrows Z$ photoreaction of CPD has been studied by using a triplet photosensitizer. On the basis of the triplet energies obtained by calculations (see Table 5), we have selected biacetyl ($E_T = 56.4$ kcal mol^{-1}) as a photosensitizer for the T_1 excited states of *E*-CPD. The complete quenching of the biacetyl phosphorescence in the condition employed for the experiments (carefully deaerated acetonitrile solutions; for more details see the Experimental Section) is an indication that quantitative energy transfer to the relevant triplet excited state of CPD takes place. Irradiation has been carried out at 420 nm, where a substantial fraction of light is absorbed by the photosenzitizer; however, direct nπ^* irradiation of CPD cannot be avoided. For this reason, the photoreaction has also been studied on the same solutions equilibrated to air, under otherwise identical experimental conditions. Since the concentration of oxygen present in the air-equilibrated solvent is largely sufficient to afford complete quenching of the photosensitizer triplet excited states, thereby switching off the photosensitized route, these experiments have been taken as a control for the direct *E*−*Z* photoisomerization of CPD.

Upon irradiation of degassed solutions containing *E*-CPD and the photosensitizer, very little spectral changes are observed, whereas irradiation of the same solutions in the presence of oxygen leads to spectral changes consistent with the $E \rightarrow Z$ isomerization, as expected for nπ^* irradiation of *E*-CPD (see Supporting Information). Taken together, these observations indicate that photosensitization of the first triplet excited state of *E*-CPD does not lead to efficient $E \rightarrow Z$ isomerization; rather,

(38) It is worth noting that the presence of different rings, namely, phenyl (ϕ) or cyclohexene (c), does not seem to affect very much the CI structures, as CIs with bigger $_c$CNN angle/smaller NNC$_f$ angle (e.g., ***Z,E*-CI$_{tors1}$** and ***Z,E*-CI$_{inv1}$**) and smaller $_c$CNN angle/bigger NNC$_f$ angle (e.g. ***Z,E*-CI$_{tors2}$** and ***Z,E*-CI$_{inv2}$**) exist (as well as with identical $_c$CNN and NNC$_f$ angles).

Scheme 4. Predicted Photoisomerization Quantum Yields for *Z*-CPD (a) and *E*-CPD (b). The Rationale Is Based on Where the Radiationless Decay Occurs along the Photochemical Reactions Channels, i.e., the Geometry of the Crossing Points (with CNNC Angles Partially or Fully Twisted) Triggering Internal Conversion[a]

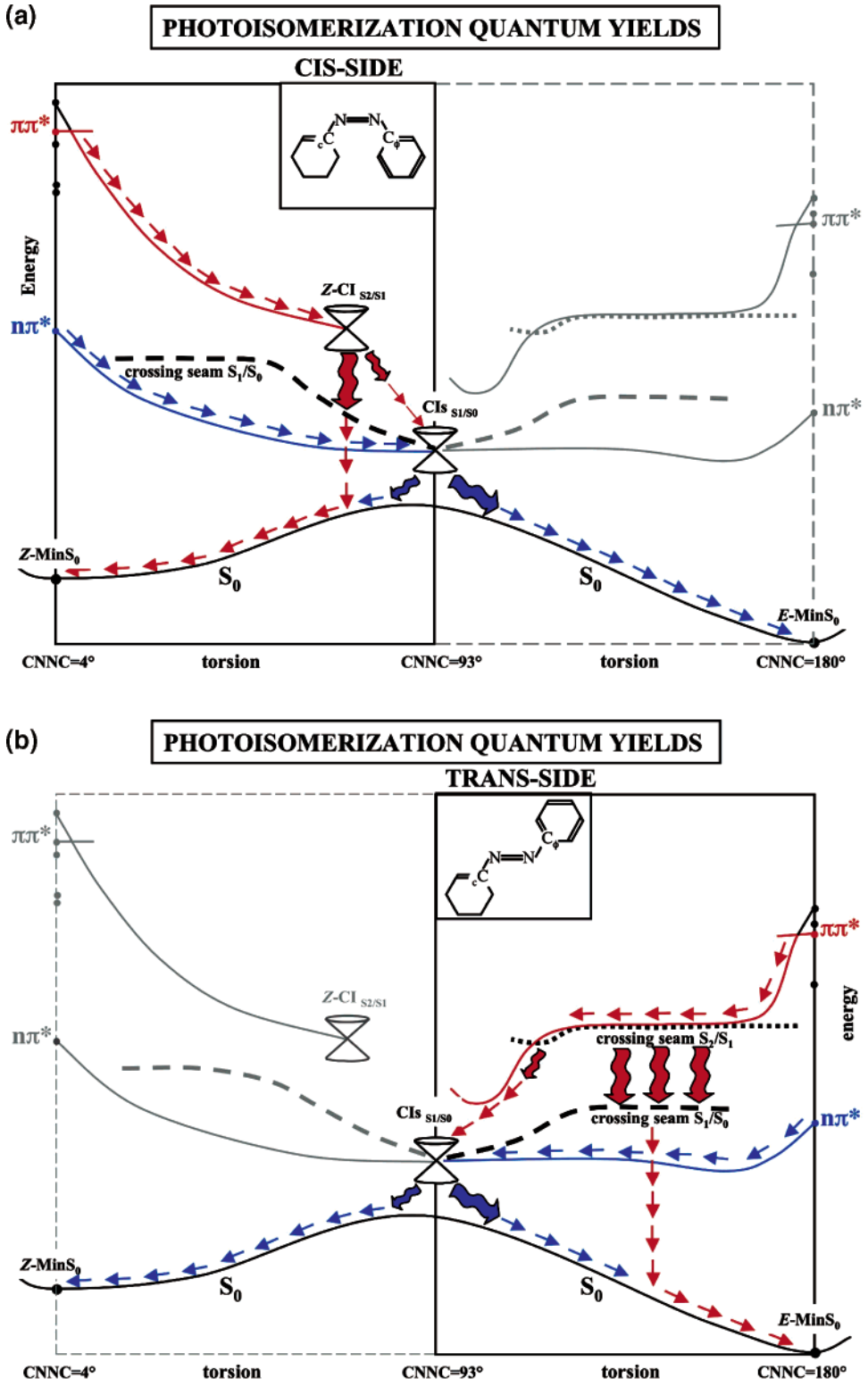

[a] Bigger arrows show the most favorite paths. The red color identifies $\pi\pi^*$ decay paths, while the blue color identifies $n\pi^*$ decay paths.

population of T_1 causes the $Z \rightarrow E$ isomerization very efficiently, thereby preventing accumulation of the *Z* isomer which is indeed formed with a substantial quantum yield (Table 4) upon direct irradiation of CPD. As it will be discussed below, this observation is consistent with the computational results.

Thermally Activated $Z \rightarrow E$ Isomerization. When a solution of *E*-CPD subjected to exhaustive irradiation at 325 nm and containing >80% of the *Z* form is left in the dark, absorption spectral changes are observed which indicate the occurrence of a back $Z \rightarrow E$ isomerization reaction. This behavior is similar

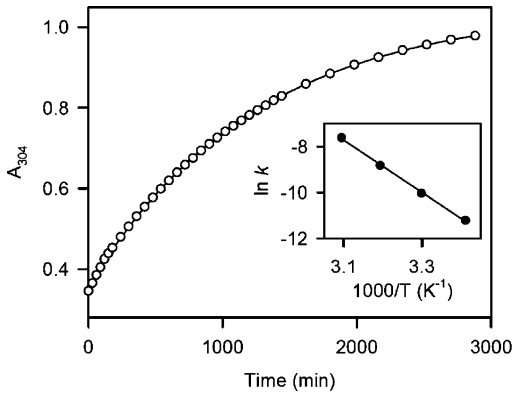

Figure 6. Absorption changes monitored at 304 nm as a function of time for an acetonitrile solution containing a mixture of *E*- and *Z*-CPD left in the dark at 20.0 °C. The starting ($t = 0$) solution was obtained by exhaustive irradiation of a 5.0×10^{-5} M solution of *E*-CPD at 325 nm. The full line represents the best fit to a first-order kinetic scheme. (Inset) Arrhenius plot shows the temperature dependence of the $Z \rightarrow E$ isomerization rate constant.

to that of azobenzene[1,2,39] and is consistent with the fact that the *E* isomer is the thermodynamically stable form of CPD. The reaction can be followed spectrophotometrically by following the recovery time of the $S_2 \leftarrow S_0$ band of the *E* isomer ($\lambda_{max} = 304$ nm). Figure 6 shows the absorption changes at 304 nm as a function of time for an acetonitrile solution of the *Z* and *E* forms (total CPD concentration, 5.0×10^{-5} M) at 20.0 °C; the inset of Figure 6 shows the temperature dependence of the rate constant (Arrhenius plot). The activation parameters obtained from the Arrhenius and Eyring equations (see Experimental Section) are gathered in Table 4. The recovery of the *E* isomer of CPD in the dark is somewhat faster compared to that of AB. It is worthwhile to note that the activation energy for the $Z \rightarrow E$ process decreases slightly on going from AB to CPD.

(39) (a) Halpern, J.; Brady, G. W.; Winkler, C. A. *Can. J. Res., Sect. B* **1950**, *28*, 140. (b) Brown, E. V.; Granneman, G. R. *J. Am. Chem. Soc.* **1975**, *97*, 621.

Table 5. CASPT2 and CASSCF Single-State Relative (ΔE) Energies for All the Relevant Points Discussed in the Text for the PES of S_0 and T_1 in CPD[a]

		CASPT2		CASSCF
structure	state	ω	ΔE (kcal mol^{-1})	ΔE (kcal mol^{-1})
***E*-MinS$_0$**	S_0	.64	0.0	0.0
	T_1	.63	48.4	62.9
	T_2	.61	65.0	71.2
***E*-MinS$_0$′**	S_0	.64	7.0	3.0
***Z*-MinS$_0$**	S_0	.64	17.8	17.0
	T_1	.63	60.5	77.5
***Z*-MinS$_0$′**	S_0	.64	17.4	16.5
Min$_{T1}$	S_0	.63	33.9	40.8
	T_1	.63	30.8	39.7
TS$_{S0}$	S_0	.63	36.5	44.0
	T_1	.63	32.6	41.2
CR1	S_0	.63	34.8	43.1
	T_1	.63	33.5	43.5
CR2	S_0	.63	29.8	35.6
	T_1	.63	31.3	40.0

[a] The energy for the ground state of the *E* form is chosen as the zero. Basis set 6-31G*. Active space: 14 electrons in 12 MOs. The weight (ω) of the zeroth order CASSCF wave function has also been reported.

The difference in the values of the preexponential factor and ΔS^* also suggest a different entropic contribution to the $Z \rightarrow E$ isomerization in the two cases.

Computational Analysis of the Isomerization in the Ground and Triplet T_1 State: S_0-T_1 Intersystem Crossing. According to CASPT2 calculations, the S_0 potential energy curve along the CNNC coordinate shows a barrier of 36.5 kcal/mol (**TS$_{S0}$**) while the T_1 potential energy curve presents a minimum (**Min$_{T1}$**) of 30.8 kcal/mol in the same twisted region (CNNC twisting of 104°); i.e. it is below the S_0 state. A qualitative picture of the S_0 and T_1 potential energy curves is shown in Figure 7 (Table 5 collects the energies of all the relevant points discussed). The two curves cross each other at about 75°(**CR1**) and 115° (**CR2**) of CNNC twisting. The energy of the former crossing, which is closer to the *Z* form, is the

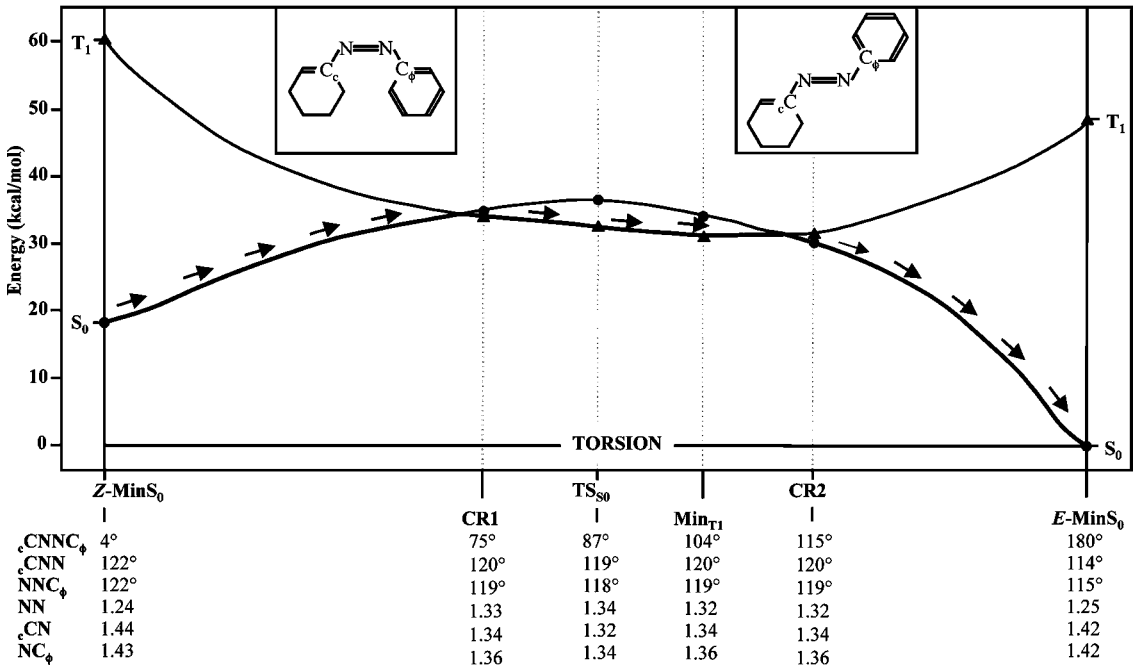

Figure 7. S_0 and T_1 potential energy profiles along the $-N{=}N-$ isomerization path. Black arrows show the $Z \rightarrow E$ thermal isomerization by the torsion mechanism via $S_0-T_1-S_0$ non-adiabatic path involving the triplet state (solid triangles). Energy profiles have been scaled to match CASPT2 values (see Table 5).

Scheme 5. Cartoonlike Drawing Summarizing *E*-CPD Photochemical Reaction Channels Triggered by nπ^* (Blue Arrows) and $\pi\pi^*$ (Red Arrows) Excitations[a]

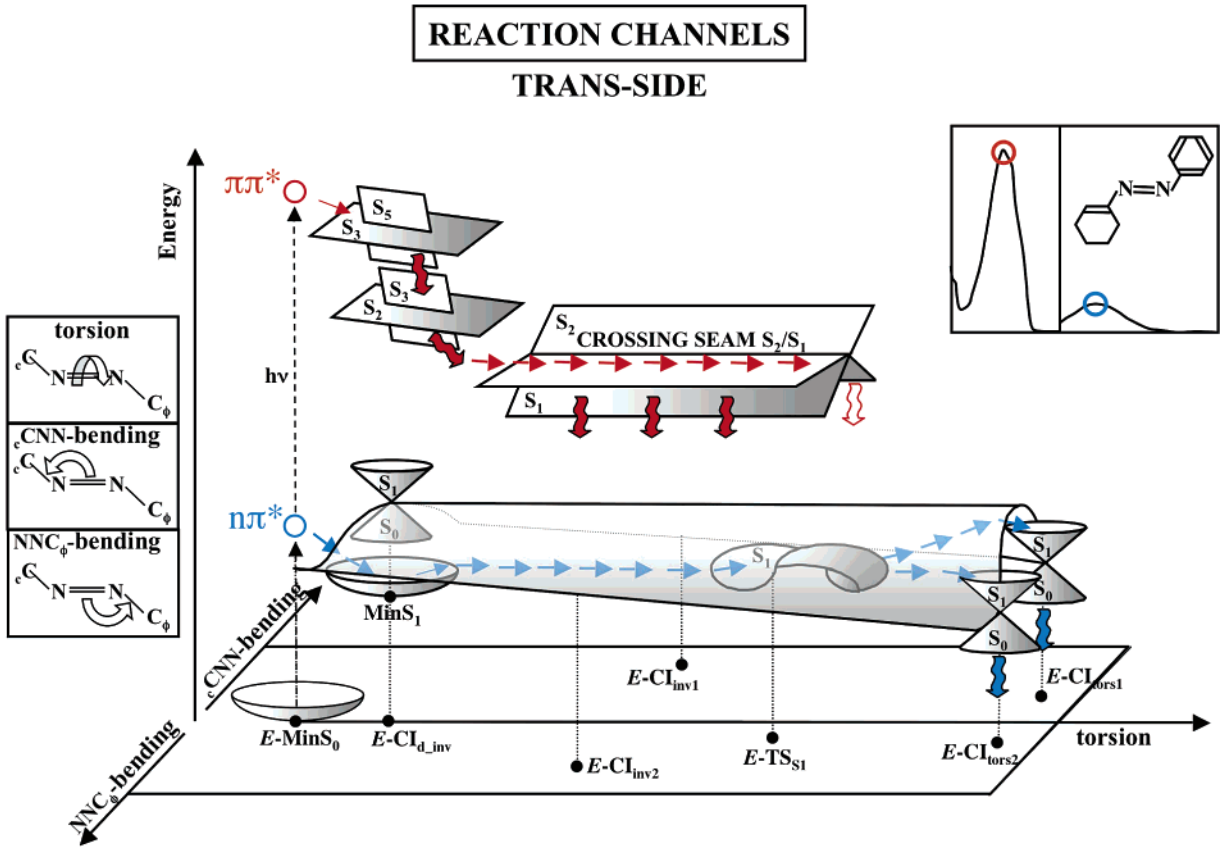

[a] The semi-transparent surface represents the S_1/S_0 crossing region: it spans very different structures along the −N=N− torsional and the asymmetric bending coordinates. Empty arrows show the less probable paths.

higher and is 34.8 kcal/mol above the *E* isomer, while the latter is 29.8 kcal/mol above the *E* isomer. Thus, CPD can easily cross from S_0 to T_1, or vice versa, in the twisted region, provided a significant S_0-T_1 spin−orbit coupling exists.

These findings support the idea that the decay of T_1 can occur more efficiently via the torsion mechanism with a rate depending on the strength of the relevant spin−orbit couplings. In our previous work on AB[18e] (which substantially presents an identical topology for the S_0 and T_1 states), we have shown that these couplings are large enough to ensure that the rate of the $T_1 \rightarrow S_0$ intersystem crossing process is of the order of 10^{11} s^{-1}. This rate indicates that AB can decay from T_1 to the ground state in a picosecond time scale and that the torsion mechanism provides indeed a very efficient mechanism for the T_1 decay and isomerization. Because of the analogy of the two systems, we suggest a similar situation for CPD with a very short T_1 lifetime that should lead to a difficult spectroscopic detection of this state.

These findings support also the idea that the thermal isomerization of CPD can proceed by the torsion mechanism via the $S_0-T_1-S_0$ non-adiabatic path involving the triplet state. Remarkably, also the calculated $Z \rightarrow E$ activation energy along this triplet-mediated path is consistent with the measured kinetic parameter. In fact, our calculated barrier (from the *Z* isomer to the higher crossing point) is 17 kcal/mol, which is in fairly good agreement with the activation enthalpy of 21.9 kcal/mol measured for the thermal isomerization. Although it may appear quite surprising that thermal isomerization does involve spin-forbidden processes (indeed, this would suggest a much smaller pre-exponential factor than the recorded one of about 10^{11} s^{-1}), we have already shown in AB[18e] that the computed S_0-T_1 spin−orbit coupling values lead to an $S_0 \rightarrow T_1$ intersystem crossing rate that is of the same size of the pre-exponential factors reported for the thermal $Z \rightarrow E$ isomerization of AB and CPD (see Table 4). Therefore, the present calculation indicates that thermal isomerization occurs by the non-adiabatic torsion mechanism and predicts kinetic parameters in agreement with the experimental results.

Interpretation of Photoisomerization Quantum Yields in the Triplet State. According to the experimental results, the *E* $\rightarrow$ *Z* photosensitized isomerization is inefficient (or does not occur at all), whereas the $Z \rightarrow E$ photosensitized process appears to be very efficient. These observations are accounted for by the fact that the lower-energy S_0/T_1 crossing (where the $T_1 \rightarrow S_0$ intersystem crossing should occur) is on the *E* side (CNNC torsion of ~104°) and is almost degenerate with the T_1 minimum (see Figure 7). Therefore, T_1 decay should always lead to the *E* isomer on the ground state, in agreement with the observations.

4. Conclusions

The main purpose of this work has been to analyze the isomerization routes of CPD in the ground and excited (nπ^* and $\pi\pi^*$) singlet states and in the triplet state by means of computational and experimental tools. By using high-level quantum chemical methods, we have searched for the photochemical reaction channels leading from the *E* and *Z* excited

Scheme 6. Cartoonlike Drawing Summarizing *Z*-CPD Photochemical Reaction Channels Triggered by nπ* (Blue Arrows) and ππ* (Red Arrows) Excitations[a]

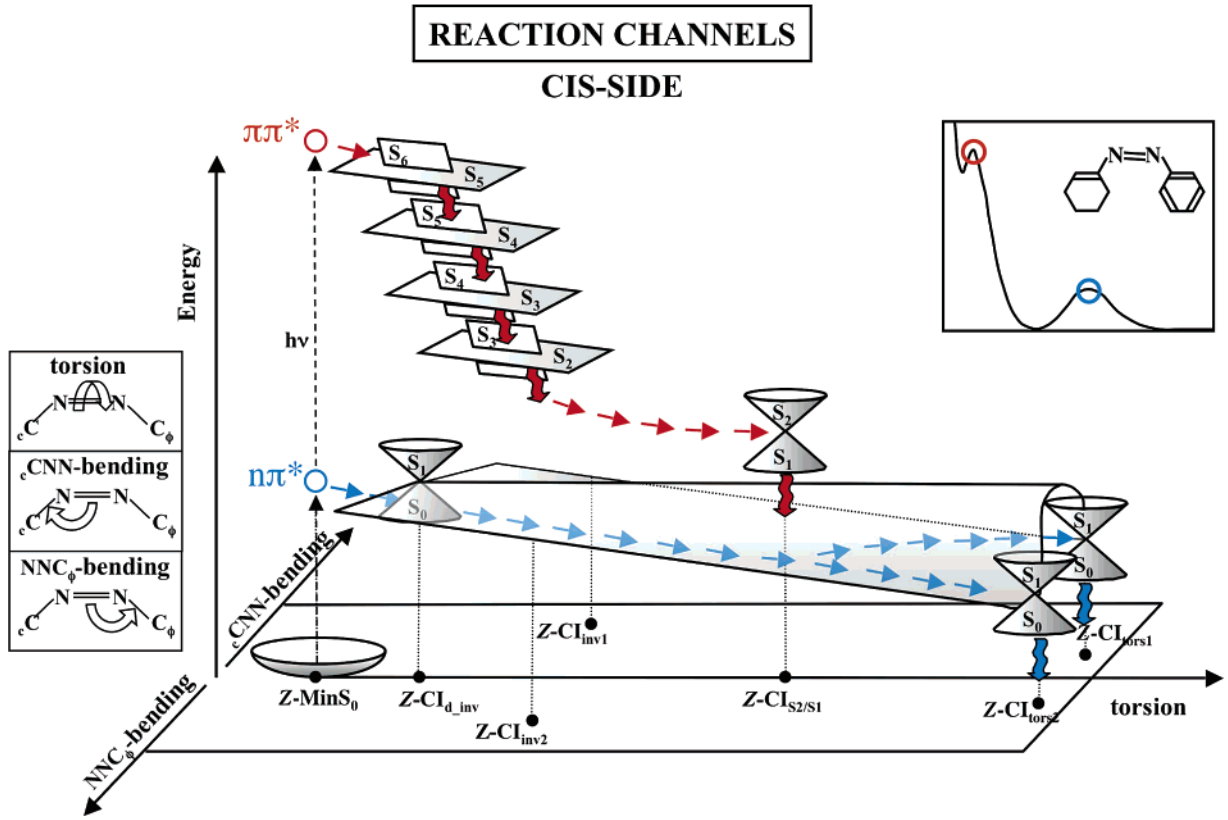

[a] The semi-transparent surface represents the S_1/S_0 crossing region: it spans very different structures along the −N═N− torsional and the asymmetric bending coordinates.

isomers to the funnels determining the decay of the system, eventually leading to the final photoproducts on the ground state. We have also matched experiments with computational predictions, finding a reasonable agreement between calculations and observations and drawing a fully comprehensive reaction scheme for the photochemistry of CPD, which accounts for the observed photophysical/photochemical properties. A cartoonlike drawing summarizing these results is reported in Scheme 5 (*E* isomer) and Scheme 6 (*Z* isomer).

To clarify further the interplay (and decay) of the photochemically relevant states involved in the reactive processes, we have mapped the S_3/S_2, S_2/S_1, and S_1/S_0 CI hyperlines connecting the different branches of the photochemical paths. The results show the existence of complex and extended intersections spaces whose accessibility and structural properties allow an understanding of the observed photochemical outcome.

In conclusion we have shown that, despite the difference in molecular structure, the photophysical and photochemical properties of CPD in the singlet and triplet states are substantially the same as those in azobenzene. Nevertheless, CPD is a better $Z \rightarrow E$ photoisomerizing system, leading to a higher (∼70%) $\Phi_{Z\rightarrow E}$ (nπ*) quantum yield. Therefore, CPD appears as a simpler but more efficient substitute of azobenzene, still retaining all its main reactivity features but with new promising functionalization opportunities. Furthermore, due to the photochemical/photophysical similarity of the two systems, CPD can be seen as a reliable model for the reactivity of azobenzene itself. In particular, because of the reduced size of its π-system compared to that of AB, CPD has been fully studied with a complete (i.e., unreduced) active space allowing highly accurate CASPT2//CASSCF mappings of the potential energy surfaces of the photochemically relevant states, and reliable computational descriptions at a level of accuracy that is currently much more expensive for AB. The computed reaction channels provide a detailed understanding of the photochemical reactivity of CPD, which is in agreement with the experiments and can be regarded as a general model for the photoreactivity of azobenzene-type compounds in general.

A similar study for AB is under way and will be presented elsewhere.

Acknowledgment. Support from the University of Bologna (funds for selected research topics), from MURST PRIN 2005 (Project: "Trasferimenti di energia e di carica a livello molecolare") and FIRB (RBAU01L2HT) are gratefully acknowledged.

Supporting Information Available: Cartesian coordinates of all the optimized structures discussed in the text, additional tables and figures and complete refs 30 and 31. This material is available free of charge via the Internet at http://pubs.acs.org.

JA0668466